Supplementary Information

Non-halogenated and Non-volatile Solid Additive for Improving the Efficiency and Stability of Organic Solar Cells

Mi Choi,‡[a] Hyeon-Seok Jeong,‡[b] Jinho Lee,[c] Yeonsu Choi,§[ad] In-Bok Kim,[b] Dong-Yu Kim,[d] Hongkyu Kang,*[b] Soo-Young Jang*[b]

[a] Heeger Center for Advanced Materials, Gwangju Institute of Science and Technology, Gwangju, 61005, Republic of Korea

[b] Research Institute for Solar and Sustainable Energies, Gwangju Institute of Science and Technology, Gwangju, 61005, Republic of Korea, gemk@gist.ac.kr, syjang@gist.ac.kr

[c] Department of Physics, Incheon National University, 119 Academy-ro, Yeonsu-gu, Incheon 22012, Republic of Korea

[d] School of Materials Science and Engineering, Gwangju Institute of Science and Technology, Gwangju, 61005, Republic of Korea

‡ M. Choi and H.-S. Jeong contributed equally to this work.

§ Current address: Advanced Energy Materials Research Center, Korea Research Institute of Chemical Technology (KRICT), 141 Gajeongro, Yuseong, Daejeon 34114, Republic of Korea

Experimental

Materials.

All reagents and solvents were purchased from commercial suppliers and used without further purification. PM6 and Y6 were purchased from 1-Material Inc. PID was synthesized via a simple two-step process, as described in Scheme S1.

Instruments and measurements.

TGA was performed using a thermogravimetric analyzer (TGA-50, Shimadzu) by heating the specimens from 25 to 900 °C at heating rates of 5 and 10 °C min^{-1}. FT-IR spectra were obtained using an FT-IR spectrometer (Vertex 70v, Bruker, USA). The UV-vis absorption spectra of all films were obtained using a UV-vis spectrophotometer (Cary 5000, Agilent). The surface morphologies of all films were characterized using atomic force microscopy (AFM) (Multimode 8, Bruker) with the AFM probe (Nanoworld, NCHR, Switzerland) in tapping mode. The Grazing incidence wide-angle X-ray scattering (GIWAXS) measurements were performed using the 9A beamline, a synchrotron radiation source, at the Pohang Accelerator Laboratory. All films were thermally annealed at 85 °C for 10 min before UV-vis absorption, AFM, and GIWAXS measurements. The TRPL spectra were recorded using a fluorescence spectrometer (FS5, Edinburgh Instruments) equipped with a time-correlated single-photon counting (TCSPC) setup, including an EPL/EPLED mount and additional TCSPC electronics. The samples were excited using a 450 nm (448 nm ±7 nm) picosecond pulsed diode laser (EPL-450, typical pulse width: 100 ps, repetition rate: 10 MHz, and intensity: 5 mW cm^{-2}). The pulse period was fixed at 50 ns during measurements. The detection wavelengths were set at 670 and 820 nm, considering the photoluminescence (PL) peaks of PM6 and Y6, respectively. The PL decay lifetime was calculated as 1/e of the initial value of the TRPL spectrum. The thermally aged samples were excited by exposing the area without covering the top electrode to ensure PL emission from the photoactive layer. ^{1}H NMR spectroscopic analysis of all compounds was performed using a 400 MHz NMR spectrometer (JNM-ECX400, Jeol). MALDI-TOF spectra were recorded using a mass spectrometer (Autoflex Speed, Bruker). Elemental analysis was performed using an elemental analyzer (UNICUBE, Elementar).

Device fabrication and characterization.

Inverted OSC devices with glass/ITO/ZnO/active layer/MoO_3/Ag structure were fabricated and characterized. The ITO-coated glass substrates were cleaned sequentially using deionized water, acetone, and isopropanol in a sonication bath for 15 min each. The substrates were further treated with ultraviolet/ozone (UV-O_3) for 20 min before solution processing. The cleaned ITO substrates were then dried in an oven for 20 min at 100 °C. Devices with ZnO as the electron transport layer were prepared by spin-coating the ZnO layer onto the UV-O_3 treated ITO substrate and annealing at 200 °C for 10 min in air. The substrates were transferred to an N_2-filled glove box in a well-controlled environment (H_2O < 1 ppm, O_2 < 3 ppm). The photoactive layer was fabricated by preparing solutions of PM6:Y6 (13.2 mg mL^{-1}) without an additive, PM6:Y6 (13.2 mg mL^{-1}) with CN (0.5 vol.%), and PM6:Y6 (13.2 mg mL^{-1}) with PID (6.1–15.3 wt.%) in chloroform. All donor-to-acceptor weight ratios were fixed at 1:1.2. After PID addition, the blend solution was stirred for over 2 h. All active layers were spin-coated onto a ZnO layer at 2,000 rpm for 25 s, then thermal annealing at 85 °C for 10 min. Subsequently, 10 nm of molybdenum oxide (MoO_3) and 100 nm of Ag were thermally evaporated onto the substrate under high-vacuum conditions to form the anode and counter cathode. Current density–voltage measurements were performed using a Keithley 2420 source meter under the AM 1.5G (100 mW cm^{-2}) irradiation provided by a Newport Oriel Sol3A Class AAA solar simulator. The light intensity was calibrated using a certified standard silicon reference solar cell (with a KG3 filter) from the National Renewable Energy Laboratory. External quantum efficiency (EQE) spectra were collected using an Oriel Quantax-300 instrument. The cell area was defined using a metal mask with an aperture area of 4.64 mm^2 to ensure the accuracy of the current density obtained from the EQE measurements.

Electron Mobility and Hole Mobility Measurements.

Electron-only devices (EOD) and hole-only devices (HOD) were fabricated with the following architectures: ITO/ZnO/active layer/PDINO/Al for electrons and ITO/ZnO/active layer/ZnO(Au) for holes. Electron and hole mobilities were extracted by fitting the current density-voltage (J-V) curves to the Mott-Gurney equation (space charge limited current). In essence, we obtained mobilities by measuring J-V curves and fitting the results to a space-charge-limited model.

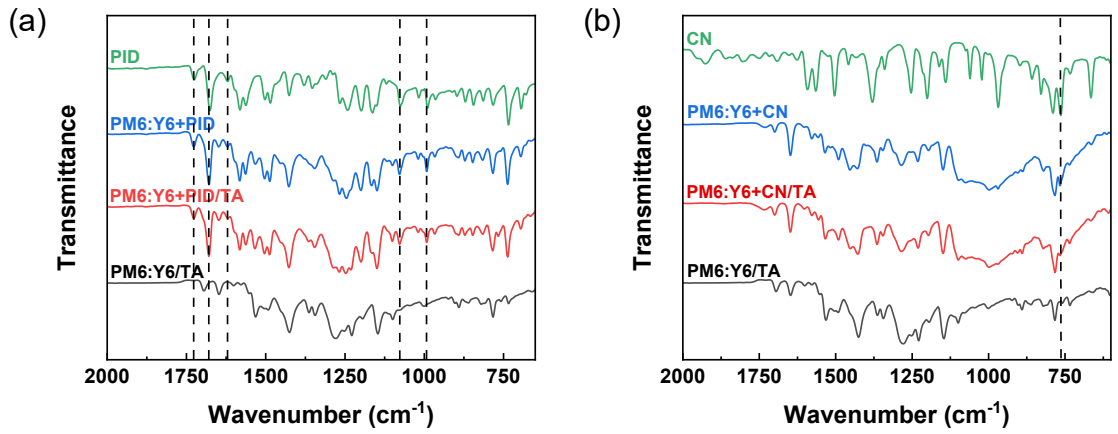

Figure S1. FT-IR spectra of (a) PM6:Y6+PID and (b) PM6:Y6+CN films with and without TA treatment at 85 ℃ for 10 min.

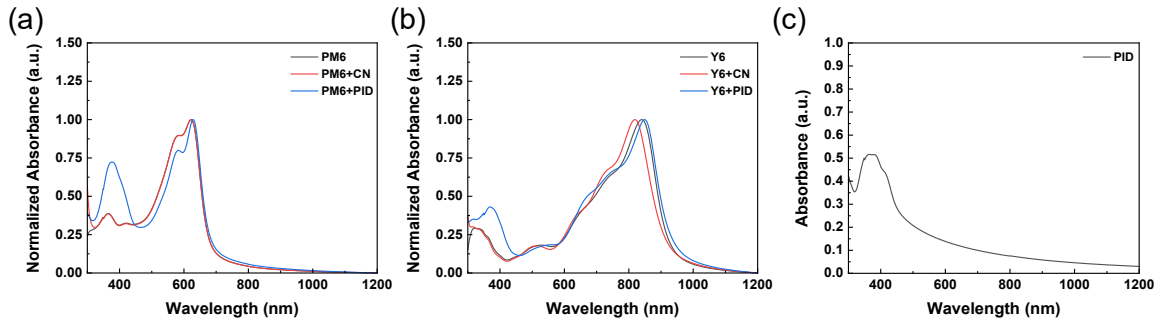

Figure S2. UV-vis absorption spectra of (a) PM6, PM6+CN, PM6+PID, (b) Y6, Y6+CN, Y6+PID, and (c) PID films after TA treatment at 85 ℃ for 10 min.

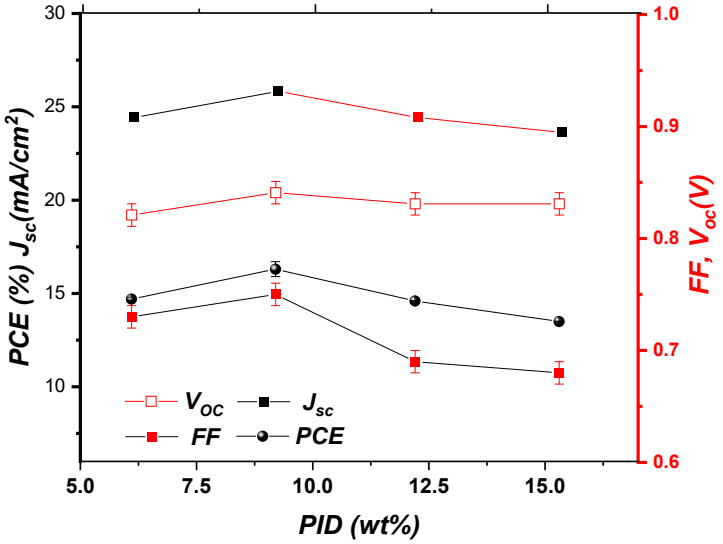

Figure S3. Photovoltaic parameters for PM6:Y6-based devices with varying quantities of PID.

Table S1. Photovoltaic parameters of PM6:Y6-based devices with varying quantities of PID

Additive	Additive Contents [%] [a]	V_{OC} [V]	J_{SC} [mA/cm^2]	J_{cal} [mA/cm^2]	FF	PCE [%][b]
PID	6.1	0.81 ± 0.01	24.2 ± 0.2	24.22 ± 0.1	0.72 ± 0.01	14.6 ± 0.1 (14.7)
	9.2	0.83 ± 0.01	25.5 ± 0.3	25.02 ± 0.2	0.74 ± 0.01	15.9 ± 0.4 (16.3)
	12.2	0.82 ± 0.01	24.2 ± 0.2	23.58 ± 0.1	0.68 ± 0.01	14.5 ± 0.1 (14.6)
	15.3	0.82 ± 0.01	23.5 ± 0.1	23.10 ± 0.2	0.67 ± 0.01	13.4 ± 0.1 (13.5)

[a] Weight ratio relative to PM6:Y6; [b] All devices were thermal annealed at 85 °C for 10 min. Average values with standard deviations were obtained from 10 devices.

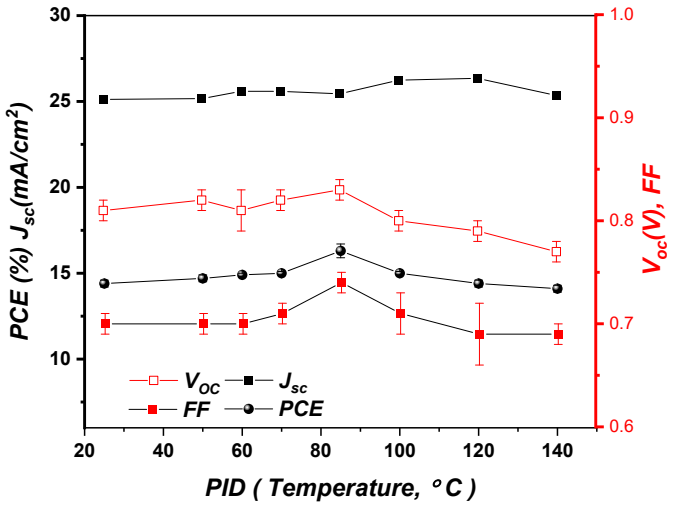

Figure S4. Photovoltaic parameters for PM6:Y6-based devices with PID at different annealing temperatures.

Table S2. Photovoltaic parameters of PM6:Y6-based devices with PID at different annealing temperatures

Additive	Annealing temperature	V_{OC} [V]	J_{SC} [mA/cm^2]	J_{cal} [mA/cm^2]	FF	PCE [%]
PID	25	0.81 ± 0.01	25.18 ± 0.1	24.63 ± 0.1	0.70 ± 0.01	14.4 ± 0.2 (14.6)
	50	0.82 ± 0.01	25.22 ± 0.1	24.75 ± 0.1	0.70 ± 0.01	14.7 ± 0.2 (14.9)
	60	0.81 ± 0.02	25.65 ± 0.1	24.81 ± 0.2	0.70 ± 0.01	14.9 ± 0.1 (15.07)
	70	0.82 ± 0.01	25.65 ± 0.2	24.90 ± 0.1	0.71 ± 0.01	15.0 ± 0.1 (15.14)
	85	0.83 ± 0.01	25.5 ± 0.3	25.02 ± 0.2	0.74 ± 0.01	15.9 ± 0.4 (16.3)
	100	0.80 ± 0.01	26.3 ± 0.2	25.50 ± 0.1	0.71 ± 0.02	15.0 ± 0.1 (15.1)
	120	0.79 ± 0.01	26.4 ± 0.3	25.83 ± 0.1	0.69 ± 0.03	14.4 ± 0.2 (14.6)
	140	0.77 ± 0.01	25.4 ± 0.3	25.80 ± 0.3	0.69 ± 0.01	13.8 ± 0.2 (14.00)

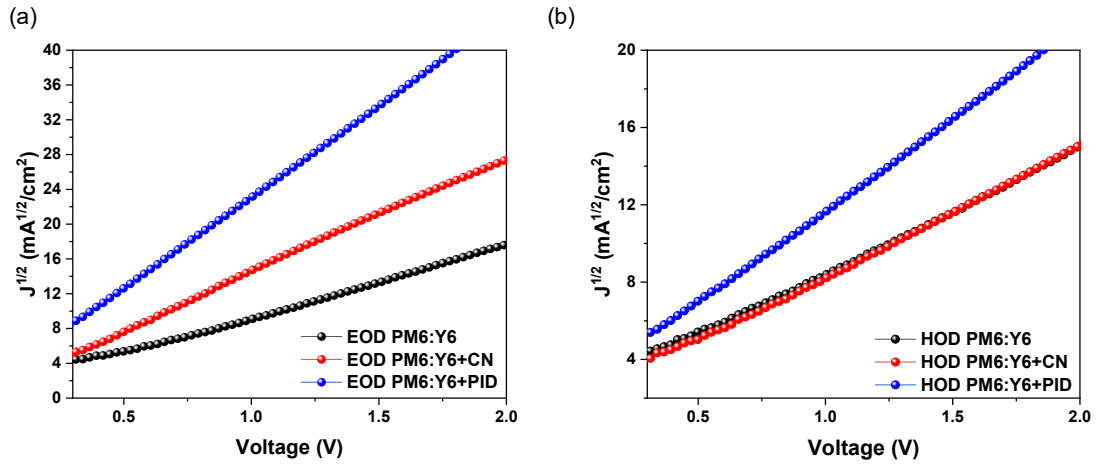

Figure S5. (a) Ln (J) versus Ln (V) plots of EOD and (b) Ln (JL^3/V^2) versus $(V/L)^{0.5}$ plots of HOD with and without additives.

Table S3. Electron and hole mobility of PM6:Y6-based devices with and without additives for SCLC measurements

Electron Mobilities ($cm^2\ V^{-1}\ s^{-1}$)		Hole Mobilities ($cm^2\ V^{-1}\ s^{-1}$)	
Condition	Electron	Condition	Hole
PM6:Y6	$2.87x10^{-4}$	PM6:Y6	$2.46\ x10^{-4}$
PM6:Y6+CN	$8.52x10^{-4}$	PM6:Y6+CN	$1.71\ x10^{-4}$
PM6:Y6+PID	$2.23x10^{-3}$	PM6:Y6+PID	$5.16\ x10^{-4}$

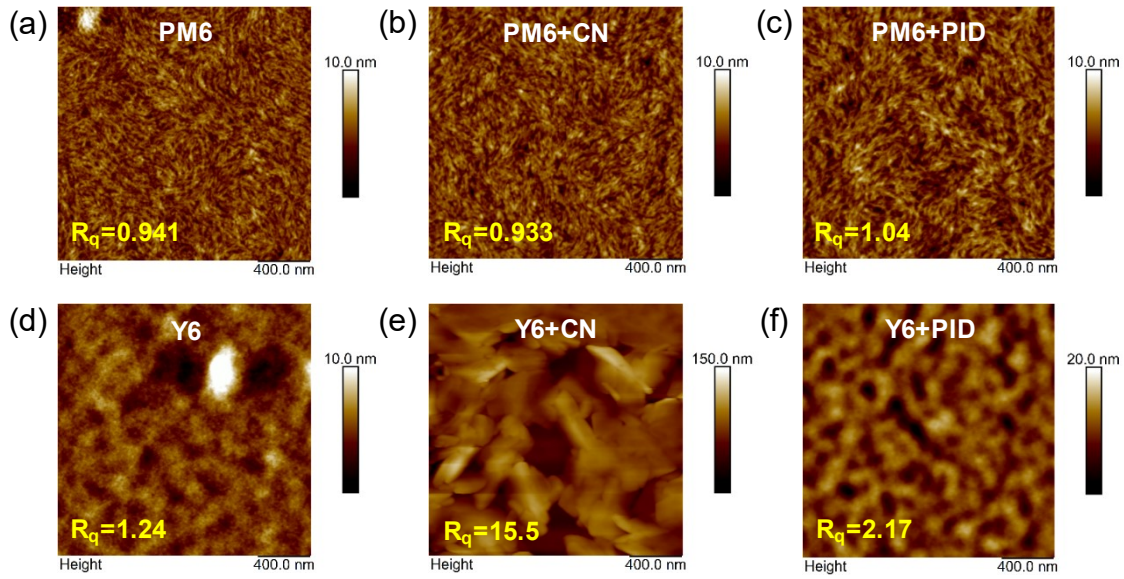

Figure S6. AFM images of neat PM6, PM6+CN, PM6+PID, and neat Y6, Y6+CN, and Y6+PID films after TA treatment at 85 ℃ for 10 min.

Table S4. The full width at half-maximum (FWHM) of the out-of-plane and corresponding π–π stacking coherence lengths (CL_{010}) for neat and blend films

Films	FWHM [$Å^{-1}$]	CL_{010} [Å]
PM6	0.396	15.848
PM6+CN	0.383	16.390
PM6+PID	0.291	21.567
Y6	0.282	22.277
Y6+CN	0.262	24.003
Y6+PID	0.203	30.877
PM6:Y6	0.261	24.074
PM6:Y6+CN	0.281	22.344
PM6:Y6+PID	0.251	28.350

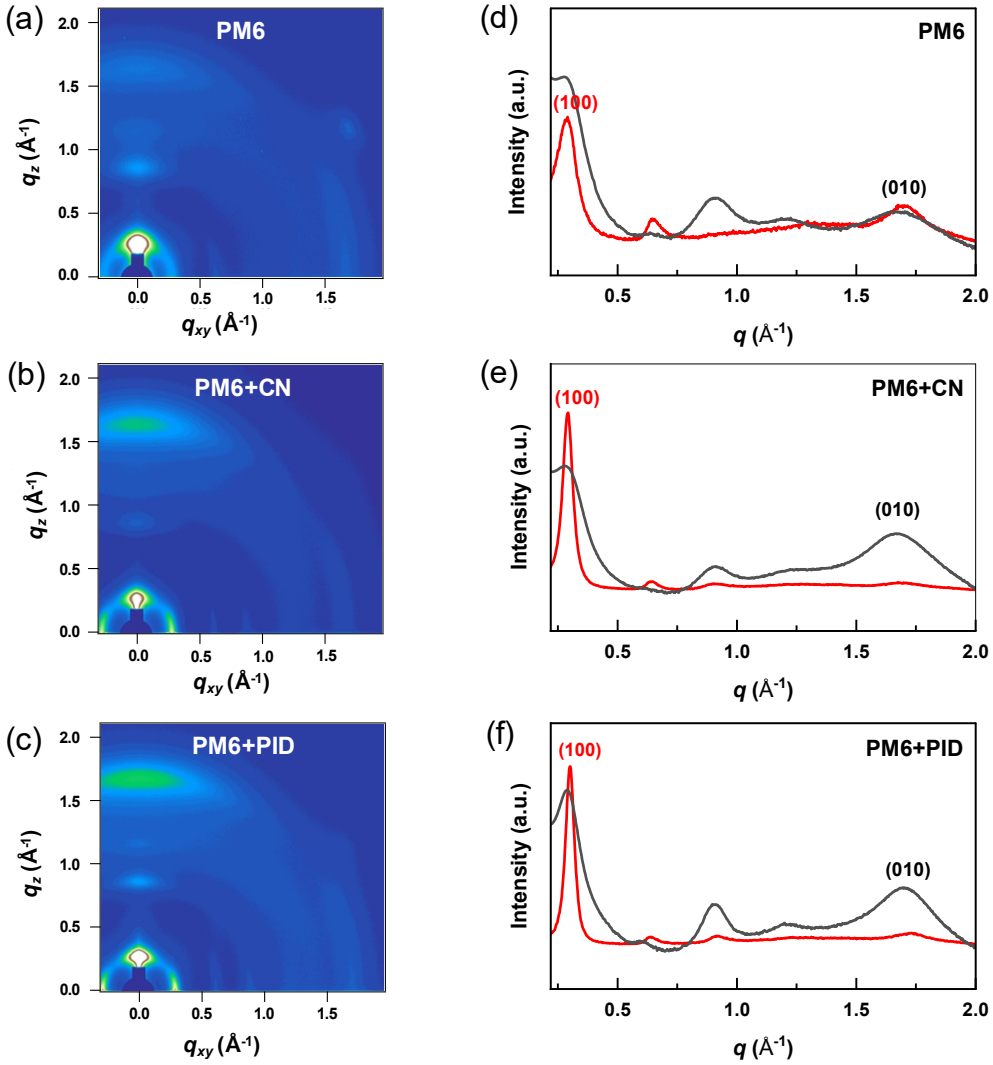

Figure S7. 2D-GIWAXS patterns of (a) PM6 (b) PM6+CN, and (c) PM6+PID. (d)–(f) The corresponding out-of-plane (black lines) and in-plane (red lines) scattering profiles of PM6 films.

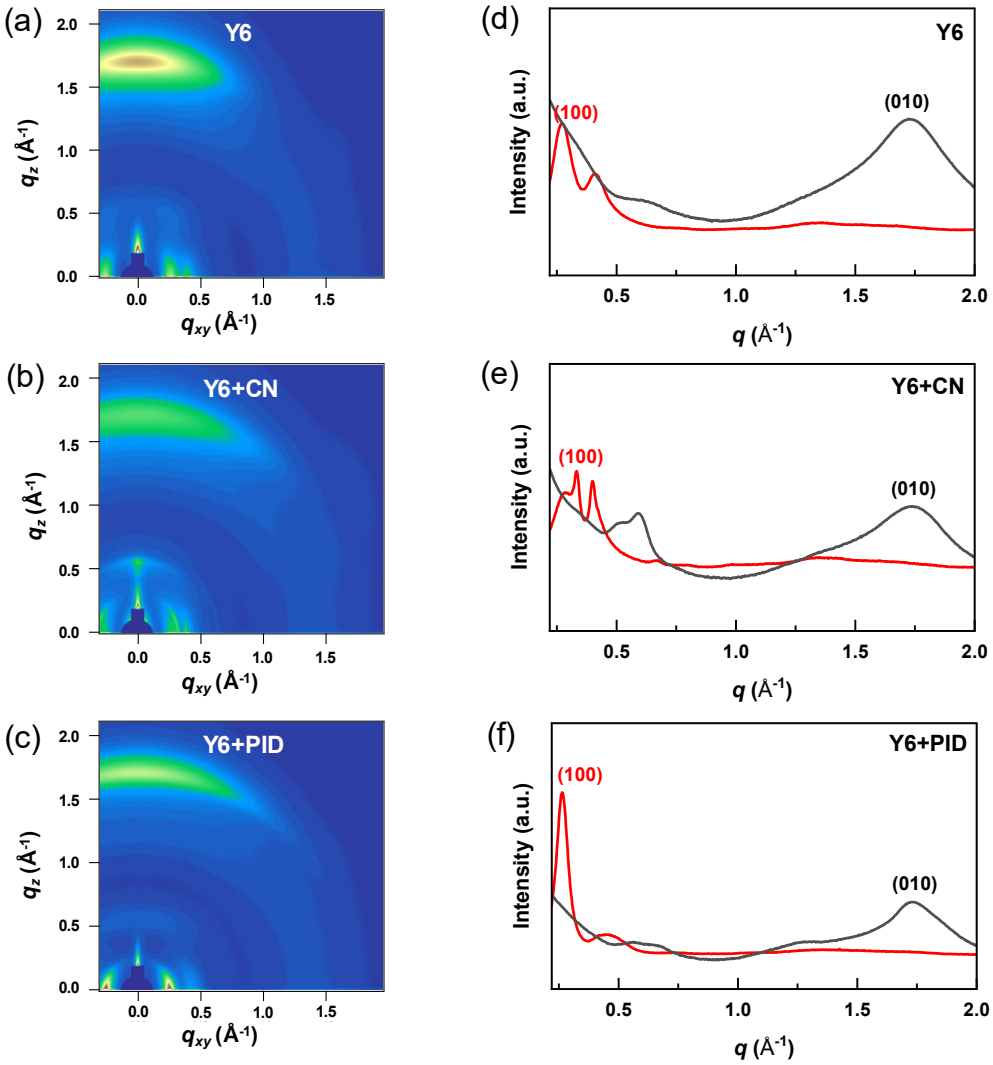

Figure S8. 2D-GIWAXS patterns of (a) Y6 (b) Y6+CN, and (c) Y6+PID. (d)–(f) The corresponding out-of-plane (black lines) and in-plane (red lines) scattering profiles of Y6 films.

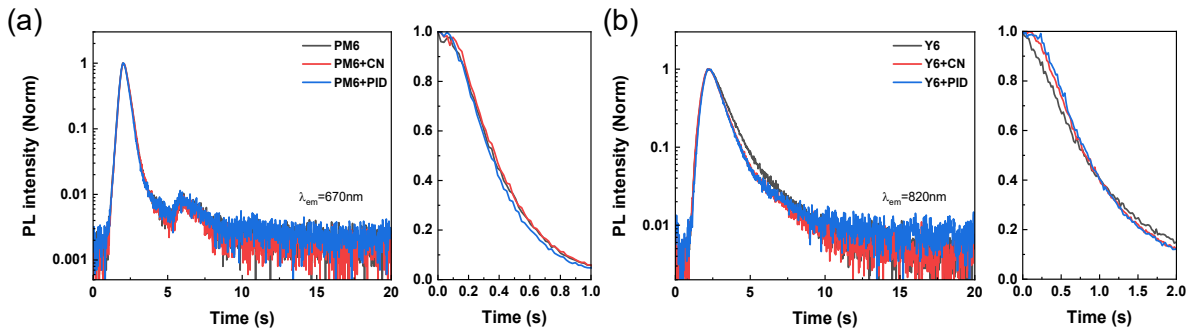

Figure S9. Normalized TRPL profiles of (a) PM6 and (b) Y6 films with and without additives. The detection wavelengths for PM6 and Y6 were set at 670 and 820 nm, respectively.

Table S5. Summary of the TRPL decay lifetimes for fresh and thermally aged PM6, Y6, and PM6:Y6 films with and without additives.

Film (fresh)	Emission [nm]	τ [ns]	Film (thermally aged[a)])	Emission [nm]	τ [ns]
PM6	670	0.46	-	-	-
PM6+CN	670	0.47	-	-	-
PM6+PID	670	0.44	-	-	-
Y6	820	1.10	-	-	-
Y6+CN	820	1.09	-	-	-
Y6+PID	820	1.07	-	-	-
PM6:Y6	670	0.45	PM6:Y6	670	0.53
PM6:Y6+CN	670	0.44	PM6:Y6+CN	670	0.50
PM6:Y6+PID	670	0.42	PM6:Y6+PID	670	0.44
PM6:Y6	820	0.43	PM6:Y6	820	0.55
PM6:Y6+CN	820	0.42	PM6:Y6+CN	820	0.59
PM6:Y6+PID	820	0.42	PM6:Y6+PID	820	0.50

[a)] The samples were taken after thermal stability measurements at 85 ℃ for 1000 h under N_2 atmosphere.

Table S6. Thermal stability of PM6:Y6-based OSCs from this study and previous studies (2020-2023).[4-13]

Device structure	Aging Temperature [℃]	PCE_{remain} [%]	Estimated Time [hr]	Atmosphere	Ref
ITO/PEDOT/PM6:Y6:CN-BBT-Cl/PNDIT-F3N/Ag	80	40	63	N_2	[1]
ITO/PEDOT/PM6:YBO-FO/PNDIT-F3N/Ag	85	70	500	N_2	[2]
ITO/PEDOT/PM6/BCF/Y6/PNDIT-F3N/Ag	65	75	550	N_2	[3]
ITO/PEDOT/PM6:TB-4Cl/PDINO/Al	100	75	110	N_2	[4]
ITO/PEDOT/PMZ2:Y6/PFN-Br/Ag	85	79	66	N_2	[5]
ITO/ZnO/PM6:Y6:In_2Se_3/MoO_3/Ag	100	80	600	N_2	[6]
TPU/ PEDOT/PM6:BAC/ PNDIT-F3N/Ag	85	81	400	-	[7]
ITO/PEDOT/PM6:Y6:MOITIC/PDINO/Al	85	81	267	N_2	[8]
ITO/ZnO/PM6:Y6:$PC_{71}BM$:SR197/MoO_3/Ag	80	85	5	-	[9]
ITO/ZnO/PM6:Y6+PM6-b-PYT6/ MoO_3/Ag	80	86	500	N_2	[10]
ITO/ZnO/PM6:Y6+PID/ MoO_3/Ag	85	83	1200	N_2	This work

Synthesis

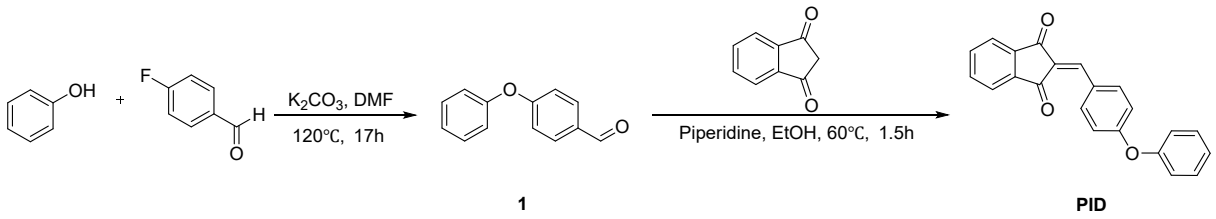

Scheme S1. Synthesis of PID.

Syntheisis of 4-phenoxybenzaldehyde (1).

4-Fluorobenzaldehyde (1.0 g, 8.00 mmol), phenol (0.83 g, 8.80 mmol), and potassium carbonate (2.30 g, 16.00 mmol) were added to DMF (10 mL). The reaction mixture was stirred at 120 °C for 16 h under an N_2 atmosphere. After cooling to room temperature, the mixture was extracted with ethyl acetate and washed with water. The organic layer was dried over $MgSO_4$ and concentrated. The crude product was purified by silica gel column chromatography using ethyl acetate/hexane (1/10, v/v). Compound 2 was obtained as a light-yellow oil (1.2 g, 75%). ^{1}H NMR (400 MHz, $CDCl_3$ with 0.05% v/v TMS): δ 9.92 (s, 1H), 7.86 (d, 2H), 7.44 (t, 2H), 7.25 (t, 1H), 7.10–7.05 (m, 4H).

Synthesis of 2-(4-phenoxybenzylidene)-1H-indene-1,3(2H)-dione (PID).

Compound 1 (1.2 g, 5.47 mmol) and 1*H*-indene-1,3(2*H*)-dione (ID, 0.80 g, 5.47 mmol) were added to ethanol (20 mL). Piperidine (0.16 mL, 1.91 mmol) was then added to this mixture. The reaction mixture was stirred at 60 °C for 1.5 h under an N_2 atmosphere and cooled to room temperature; subsequently, the solvent was concentrated. The reaction mixture was poured into ethanol and stirred for 30 min. The resulting dark-yellow precipitate was filtered and washed with ethanol. The precipitate was dissolved in dichloromethane (30 mL) and filtered again. The filtrate was concentrated, and the crude product was recrystallized with dichloromethane and ethanol. PID was obtained as a bright-yellow solid (1.14 g, 71.2% yield). ^{1}H NMR (400 MHz, $CDCl_3$ with 0.05% v/v TMS): δ 8.53 (d, 2H), 8.01–7.99 (m, 2H), 7.86 (s, 1H), 7.82–7.79 (m, 2H), 7.44 (t, 2H), 7.25 (t, 1H), 7.13 (d, 2H), 7.07 (d, 2H); MS (MALDI-TOF) *m/z*: calcd for $C_{22}H_{14}O_3$, 326.09; found, 326.5. Elemental analysis; predicted: C = 80.97, H = 4.32, and O = 14.71; found: C = 80.90, H = 4.19, and O = 14.75.

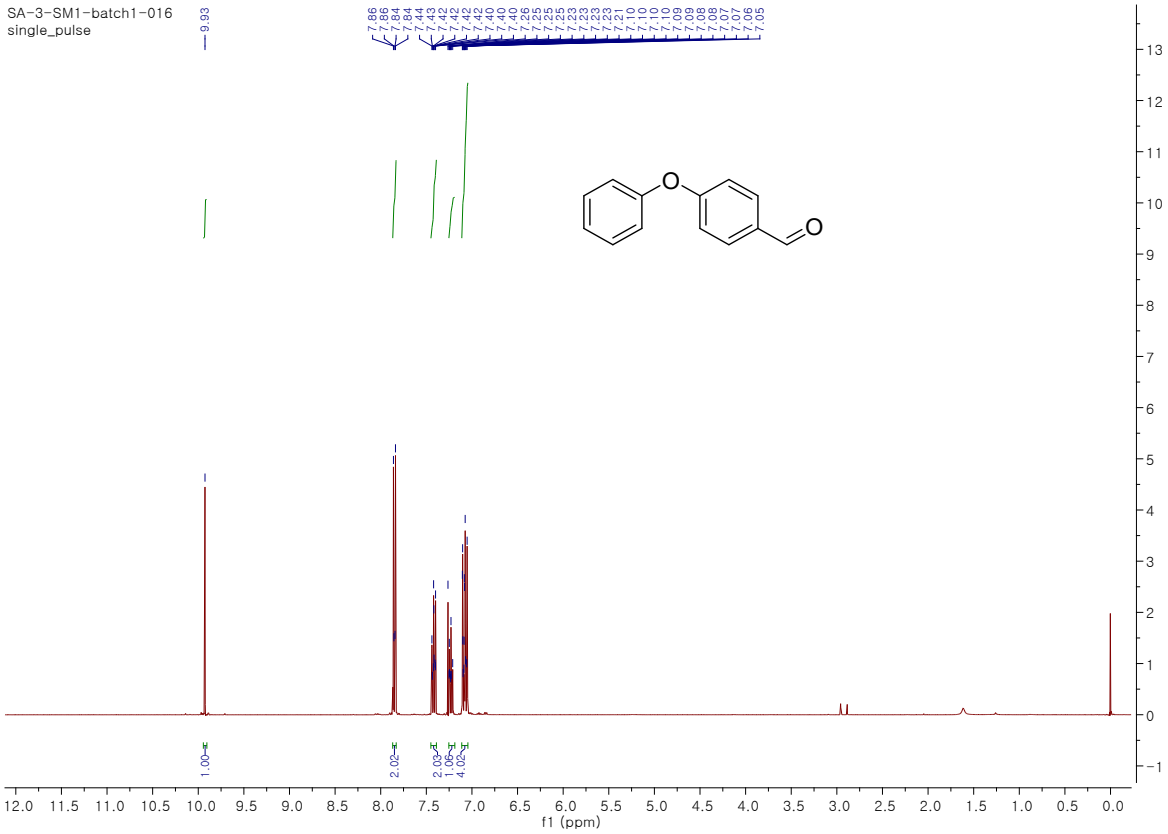

Figure S10. ^{1}H NMR spectrum of 4-phenoxybenzaldehyde (1).

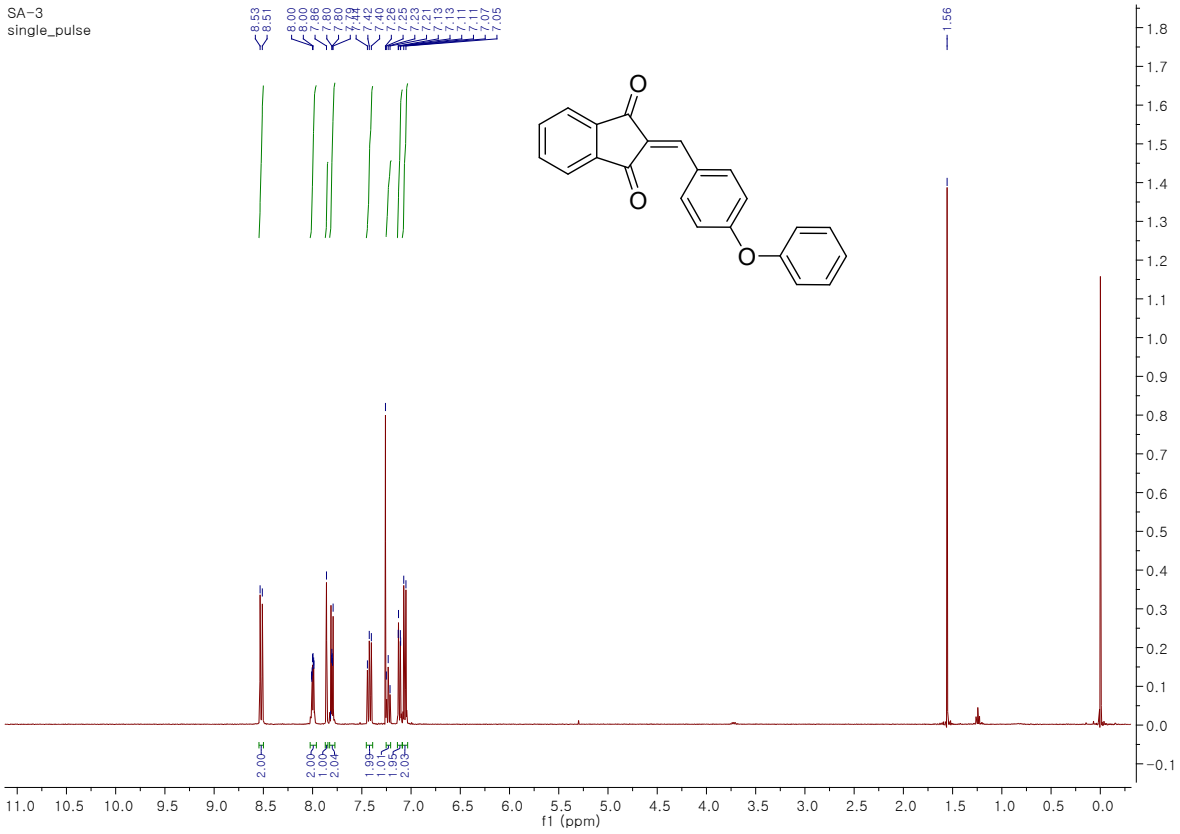

Figure S11. ^{1}H NMR spectrum of 2-(4-phenoxybenzylidene)-1*H*-indene-1,3(2*H*)-dione (PID).

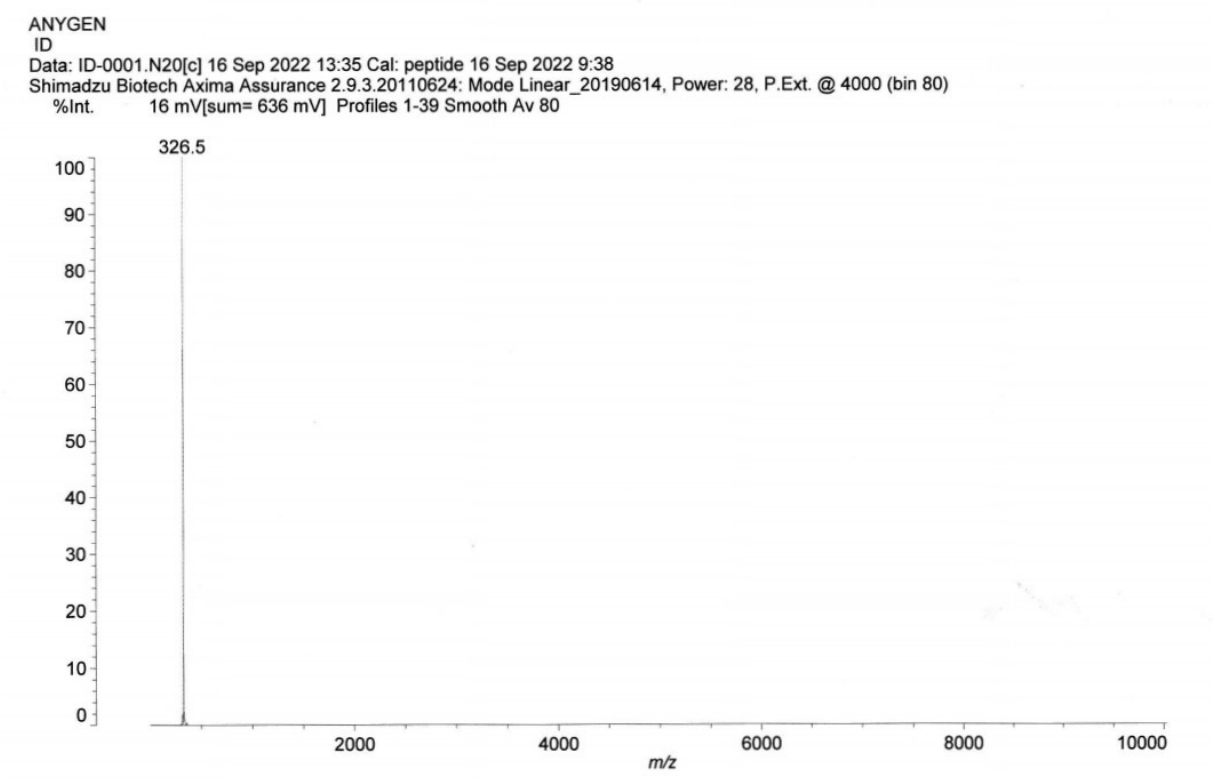

Figure S12. MALDI-TOF spectrum of 2-(4-phenoxybenzylidene)-1*H*-indene-1,3(2*H*)-dione (PID).

Supplementary References

1 Y.-N. Yang, X.-M. Li, S.-J. Wang, X.-P. Duan, Y.-H. Cai, X.-B. Sun, D.-H. Wei, W. Ma, Y.-M. Sun, *Chinese Journal of Polymer Science*, 2023, **41**, 194-201.

2 D. Yuk, M.H. Jee, C.W. Koh, W.-W. Park, H.S. Ryu, D. Lee, S. Cho, S. Rasool, S. Park, O.-H. Kwon, J.Y. Kim, H.Y. Woo, *Small*, 2023, **19**, 2206547.

3 H. Zhang, X. Zhang, Y. Li, G. Huang, W. Du, J. Shi, B. Wang, S. Li, T. Jiang, J. Zhang, Q. Cheng, J. Chen, B. Han, X. Liu, Y. Zhang, H. Zhou, *Solar RRL*, 2022, **6**, 2101096.

4 J. Zhang, Y. Han, W. Zhang, J. Ge, L. Xie, Z. Xia, W. Song, D. Yang, X. Zhang, Z. Ge, *ACS Appl. Mater. Interfaces*, 2020, **12**, 57271-57280.

5 J. Wu, X. Guo, M. Xiong, X. Xia, Q. Li, J. Fang, X. Yan, Q. Liu, X. Lu, E. Wang, D. Yu, M. Zhang, *Chemical Engineering Journal*, 2022, **446**, 137424.

6 B. Chang, H.-W. Cheng, Y.-C. Lin, H.-C. Wang, C.-H. Chen, V.-T. Nguyen, Y. Yang, K.-H. Wei, *ACS Appl. Mater. Interfaces*, 2020, **12**, 55023-55032.

7 Z. Wang, D. Zhang, M. Xu, J. Liu, J. He, L. Yang, Z. Li, Y. Gao, M. Shao, *Small*, 2022, **18**, 2201589.

8 M. Xiong, J. Wu, Q. Fan, Q. Liu, J. Lv, X. Ou, X. Guo, M. Zhang, *Org. Electron.*, 2021, **96**, 106227.

9 X. Li, L. Zhou, X. Lu, L. Cao, X. Du, H. Lin, C. Zheng, S. Tao, *Materials Chemistry Frontiers*, 2021, **5**, 3850-3858.

10 B. Li, Q. Zhang, S. Li, X. Yang, F. Yang, Y. Kong, Y. Li, Z. Wu, W. Zhang, Q. Zhao, Y. Zhang, H. Young Woo, J. Yuan, W. Ma, *Chemical Engineering Journal*, 2022, **438**, 135543.